environmental microbiology

Environmental Microbiology (2021) **23**(7), 3825–3839 doi:10.1111/1462-2920.15440

Special Issue Article

Microbial diversity and activity in Southern California salterns and bitterns: analogues for remnant ocean worlds

Benjamin Klempay,[1*] **Nestor Arandia-Gorostidi**,[2] **Anne E. Dekas**,[2] **Douglas H. Bartlett**,[1] **Christopher E. Carr**,[3,4] **Peter T. Doran**,[5] **Avishek Dutta**,[1] **Natalia Erazo**,[1] **Luke A. Fisher**,[1] **Jennifer B. Glass**,[4] **Alexandra Pontefract**,[6] **Sanjoy M. Som**,[7] **Jesse M. Wilson**,[1] **Britney E. Schmidt**[4] **and Jeff S. Bowman**[1]

[1]*Scripps Institution of Oceanography, University of California San Diego, La Jolla, CA, 92037.*

[2]*Department of Earth System Science, Stanford University, Stanford, CA, 94305.*

[3]*Daniel Guggenheim School of Aerospace Engineering, Georgia Institute of Technology, Atlanta, GA, 30332.*

[4]*School of Earth and Atmospheric Studies, Georgia Institute of Technology, Atlanta, GA, 30332.*

[5]*Department of Geology and Geophysics, Louisiana State University, Baton Rouge, LA, 70803.*

[6]*Department of Biology, Georgetown University, Washington, DC, 20057.*

[7]*Blue Marble Space Institute of Science, Seattle, WA, 98154.*

Summary

Concurrent osmotic and chaotropic stress make $MgCl_2$-rich brines extremely inhospitable environments. Understanding the limits of life in these brines is essential to the search for extraterrestrial life on contemporary and relict ocean worlds, like Mars, which could host similar environments. We sequenced environmental 16S rRNA genes and quantified microbial activity across a broad range of salinity and chaotropicity at a Mars-analogue salt harvesting facility in Southern California, where seawater is evaporated in a series of ponds ranging from kosmotropic NaCl brines to highly chaotropic $MgCl_2$ brines. Within NaCl brines, we observed a proliferation of specialized halophilic Euryarchaeota, which corresponded closely with the dominant taxa found in salterns around the world. These communities were characterized by very slow growth rates and high biomass accumulation. As salinity and chaotropicity increased, we found that the $MgCl_2$-rich brines eventually exceeded the limits of microbial activity. We found evidence that exogenous genetic material is preserved in these chaotropic brines, producing an unexpected increase in diversity in the presumably sterile $MgCl_2$-saturated brines. Because of their high potential for biomarker preservation, chaotropic brines could therefore serve as repositories of genetic biomarkers from nearby environments (both on Earth and beyond) making them prime targets for future life-detection missions.

Received 16 November, 2020; revised 12 February, 2021; accepted 15 February, 2021. *For correspondence. E-mail bklempay@ucsd.edu; Tel. 1-406-396-4621.

Introduction

Hypersaline brines are of unique astrobiological relevance due to the ubiquity of dissolved salts in contemporary ocean worlds from Earth to Enceladus, and as the source of evaporite deposits on relict ocean worlds such as Mars. These brines both constrain the habitability of aqueous environments (e.g. via osmotic and chaotropic stress) and can expand the circumstellar habitable zone by depressing the freezing point of liquid water and elevating its boiling point. Studying the limits of life in hypersaline environments is, therefore, key to understanding the extent of Earth's habitability, and by extension, whether other bodies in our Solar System or beyond could host habitable environments. Specifically, evaporative brine systems (e.g. salterns and naturally occurring salt lakes) serve as terrestrial analogues of Mars's ancient receding oceans, which could have been among the last refugia of life as the planet transitioned from wet to dry (Tosca *et al*., 2008; Altheide *et al*., 2009; Nazari-Sharabian *et al*., 2020). Because these environments

© 2021 Society for Applied Microbiology and John Wiley & Sons Ltd.

may have a high potential for biosignature preservation, they are prime habitats for life detection missions that can be guided by advanced knowledge of halophile ecology and physiology (Fredrickson *et al*., 1997; Fernández-Remolar *et al*., 2013).

Life in evaporative hypersaline systems must adapt to constantly changing salt chemistries and increasingly extreme physiochemical stresses. As water evaporates and dissolved salts become more concentrated, the water activity (a_w) of the remaining brine drops, thereby limiting the availability of free water molecules (a fundamental limitation for all life on Earth). In prokaryotes, active microbial growth has only been observed down to $a_w = 0.635$, though certain extremely xerophilic fungi are capable of cellular division down to $a_w = 0.585$, the current known water activity limit of life (Stevenson *et al*., 2015, 2017). As evapoconcentration continues, this osmotic stress (i.e. low water activity) can be accompanied by additional stressors. In evaporative systems derived from seawater, a critical shift in brine chemistry occurs as NaCl reaches its saturation point and begins to precipitate as halite. The remaining solution becomes dominated by $MgCl_2$. Life in these bittern brines must contend not only with extremely low water activity but also with chaotropicity: the disruptive effects of dissolved ions on proteins, lipid membranes and other macromolecules. Chaotropic solutes, like $MgCl_2$, destabilize and denature biomolecules by disrupting hydrogen bonding and other non-covalent molecular interactions (Sawyer and Puckridge, 1973; Duda *et al*., 2004; Cray *et al*., 2013; Ball and Hallsworth, 2015). Previous studies estimate that the chaotropic effects of $MgCl_2$ are prohibitive of life at concentrations above 2.3 M, though compensating kosmotropic (stabilizing) solutes may allow life up to 3.03 M $MgCl_2$ (Hallsworth *et al*., 2007; Yakimov *et al*., 2015). The most chaotolerant fungi known to date can grow *in vitro* up to 2.1 M $MgCl_2$ in the absence of compensating kosmotropes (Zajc *et al*., 2014). How (and to what extent) life can adapt to chaotropic stress remains poorly understood, despite evidence that chaotropicity rather than water activity defines the habitable window in $MgCl_2$-rich hypersaline environments (Hallsworth *et al*., 2007).

In this study, we describe and quantify changes undergone by the microbial communities in Southern California salterns and bitterns in response to decreasing water activity and increasing chaotropicity. South Bay Salt Works (SBSW) is a solar salt harvesting facility in Chula Vista, California (32.6° N, 117.1° W) where water from the San Diego Bay is evaporated in a series of shallow ponds to harvest NaCl and $MgCl_2$ salts (Fig. 1). Both the Mg^{2+}/Na^+ ratio and the total salt concentration increase throughout this process, and thus the salt ponds at SBSW range from kosmotropic seawater to highly chaotropic $MgCl_2$ brines. We used 16S rRNA gene amplicon sequencing and nanoscale Secondary Ion Mass Spectrometry (nanoSIMS) to explore microbial diversity and activity along the water activity and chaotropicity gradients in SBSW brines.

Results and discussion

Evapoconcentration of seawater

In order to correlate microbial diversity with the various environmental gradients present within the SBSW brines, we measured geochemical parameters and dissolved ion concentrations at each sampling site (Table 1). These measurements reveal multiple ecologically relevant geochemical gradients across the brines including a_w (0.39–0.94), pH (5.30–8.16) and Mg^{2+}/Na^+ ratio (0.234–30.15), a proxy for chaotropicity in this system. Across the SBSW brines, water activity correlated almost perfectly, albeit non-linearly, with pH (Spearman's $\rho = 0.98$; $p < 0.001$) and Mg^{2+}/Na^+ ($\rho = -1$; $p < 0.001$). Thus, we use water activity hereafter as a proxy for the other variables and the primary explanatory variable for changes in microbial diversity and composition. However, it is likely that each of these environmental parameters at least partially motivates shifts in the microbial community.

We verified the trends observed in our *in situ* measurements against numerical results of modelling seawater evaporation at thermodynamic equilibrium (Harvie *et al*., 1984). *In situ* measurements of water activity, pH and Mg^{2+}/Na^+ aligned closely with the values predicted by our theoretical calculations, confirming that SBSW is representative of thalassic (seawater-derived) evaporative systems (Fig. 2). The discrepancies in pH versus water activity between model results and *in situ* values were due to seawater being naturally supersaturated in carbonate, whereas supersaturation is not allowed in numerical equilibrium thermodynamics.

We identified three qualitatively distinct environments of interest within SBSW. First, the conduit (Site 2), which delivers seawater to the various evaporation ponds, was the least concentrated (approximately three times the salinity of standard seawater (TDS $\sim$110 g L^{-1})). Second, the halite-precipitating NaCl brines (i.e. salterns; Sites 1, 3 and 6–8) were hypersaline (TDS $\sim$300–370 g L^{-1}), slightly acidic (pH $\sim$6–7) and had a pink appearance resulting from the presence of carotenoid-containing haloarchaea. Finally, the $MgCl_2$ brines (i.e. bitterns; Sites 4 and 5)

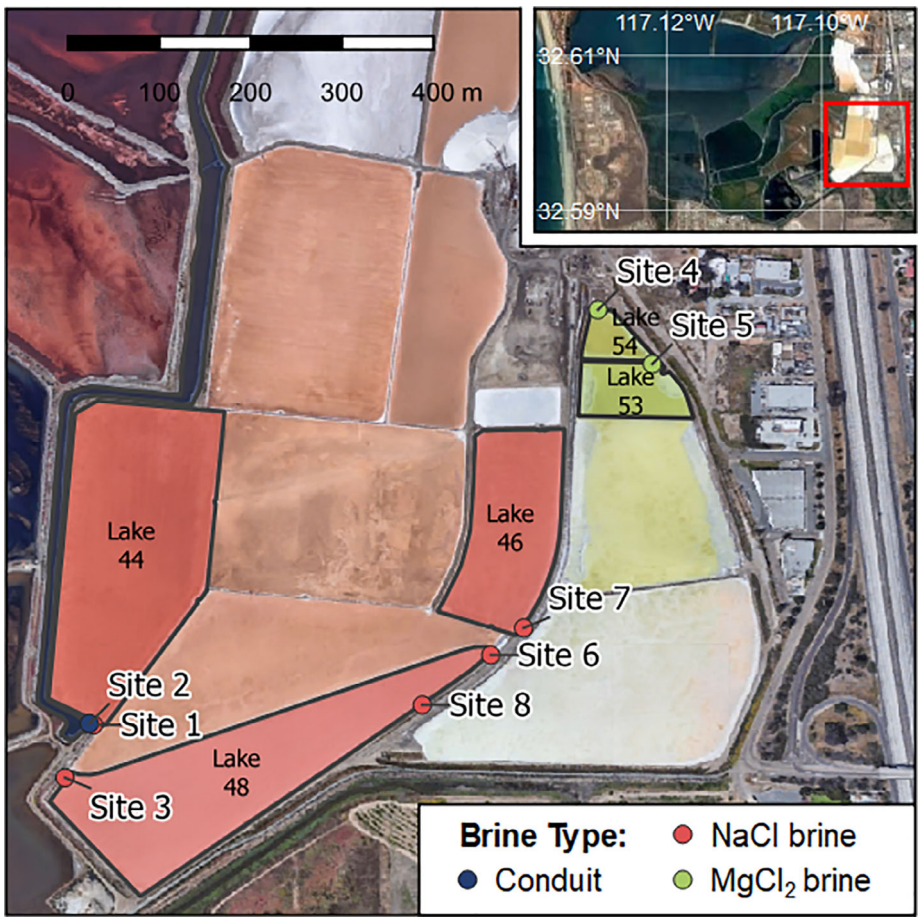


Fig 1. Map of SBSW. Inlay shows the position of our study site within SBSW, located at the South end of the San Diego Bay, Chula Vista, CA. Satellite imagery from Google Earth. [Color figure can be viewed at wileyonlinelibrary.com]

Table 1. *In situ* geochemical measurements and major ion concentrations.

Site	Brine Type	a_w	pH	[Na^+] (M)	[Mg^{2+}] (M)	[Cl^-] (M)	[SO_4^{2-}] (M)	TDS (g L^{-1})
1	NaCl	0.70	6.97	2.75	1.70	4.99	0.57	352
2-surface	Conduit	0.94	8.16	1.17	0.28	1.72	0.12	109
2-bottom	Conduit	0.94	8.03	1.18	0.29	1.76	0.13	112
3	NaCl	0.64	6.44	1.38	2.99	5.53	0.44	370
4	$MgCl_2$	0.39	5.30	0.14	4.20	7.56	0.23	403
5	$MgCl_2$	0.49	5.70	0.31	4.69	6.91	0.22	400
6	NaCl	0.68	6.83	2.13	2.09	4.94	0.70	360
7	NaCl	0.71	6.96	2.85	1.59	3.95	0.42	298
8	NaCl	0.68	6.68	2.31	2.36	4.94	0.72	375

Sites were classified into three distinct brine types: NaCl brines, $MgCl_2$ brines and the conduit, which deliver seawater to the various evaporation ponds. Total dissolved solids (TDS) were calculated by summing all ion concentrations. For complete geochemical measurements, see Supplementary Tables S1–S3.

were the most-concentrated brines at SBSW (even saltier (TDS ~400 g L^{-1}) and more acidic (pH < 6) than the NaCl brines). They were further characterized by a greenish appearance and extreme chaotropicity ($Mg^{2+}/Na^+ > 15$). $MgCl_2$-saturated brines were presumed to be devoid of active life, as $MgCl_2$ concentrations (>3.45 M) and water activity ($a_w < 0.5$) in these brines were well outside the bounds of currently established limits for metabolic activity and cellular division (Hallsworth *et al*., 2007; Oren, 2011; Stevenson *et al*., 2015; Yakimov *et al*., 2015). Still, they were included in our analysis of microbial activity in order to test this assumption. Hereafter, we describe $MgCl_2$-saturated brines as 'presumably sterile', with the following caveat: it remains possible that rare spores could persist in chaotropic brines (despite extreme physiological stress) while waiting for more

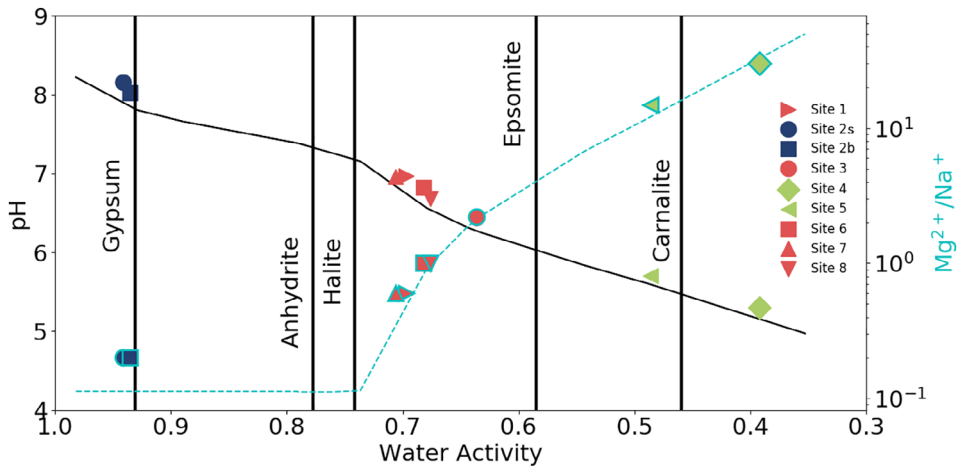


Fig 2. Geochemical parameters of SBSW brines versus theoretical seawater evaporation. Water activity is shown decreasing left-to-right from 1 (a_w of pure water). Points show empirically determined geochemical parameters for each site. Solid and dotted lines show our model predictions for (respectively) pH and Mg^{2+}/Na^{+} ratio against water activity, based on the theoretical evaporation of standard seawater. Bold vertical lines show the a_w values at which various evaporite minerals begin to precipitate from the brine. [Color figure can be viewed at wileyonlinelibrary.com]

hospitable conditions for growth (Sass *et al*., 2008; Oren, 2013; Cubillos *et al*., 2019).

Changes in microbial community composition

To quantify and describe the microbial diversity along these geochemical gradients, we purified DNA from brine samples taken at each site and sequenced 16S rRNA genes in these samples ($n = 49$) using high-throughput amplicon sequencing (Illumina). In total, 1246 unique amplicon sequence variants (ASVs) were found across the various sites at SBSW (Fig. 3). Hierarchical clustering of the microbial communities based on ASV relative abundances shows that samples clustered by brine type (conduit, NaCl brines and $MgCl_2$ brines) with high fidelity (analysis of similarities (ANOSIM); $p < 0.001$). These results are consistent with our geochemical measurements and validate our decision to divide SBSW brines into those three brine types for further factor-based analyses. Within brine types, samples clustered by site ($p < 0.001$). Moreover, we observed no major differences between samples filtered *in situ*, those collected in plastic bottles and filtered back in the lab ('_lab') and those concentrated using a concentrating pipette ('_CP_0.2' and '_CP_ULT'). This suggests that our sampling and filtration methods did not significantly bias our DNA analysis ($p = 0.788$). See Experimental procedures for detailed methods.

The composition of major taxa in our study mirrored the results of previous environmental DNA studies of SBSW brines, and closely resembled the prokaryotic communities of thalassic hypersaline brines around the world (Rodriguez-Brito *et al*., 2010; Narasingarao *et al*., 2012; Zhaxybayeva *et al*., 2013); SBSW salterns and bitterns were dominated by halophilic Euryarchaeota in the class Halobacteria (hereafter haloarchaea) (in particular, *Haloquadratum walsbyi* (by far the most abundant single taxon), *Halorubrum* and *Halohasta*). The only bacteria present in high abundance across all the various hypersaline brines was *Salinibacter ruber* (the second most abundant taxon after *H. walsbyi* (not found in high abundance in the conduit)). These cosmopolitan halophiles are globally abundant in hypersaline environments, particularly solar salterns, with *H. walsbyi* and *S. ruber* commonly accounting for over 75% of cells in NaCl-saturated brines around the world (Antón *et al*., 2002; Bolhuis *et al*., 2006; Oh *et al*., 2010). *Haloquadratum walsbyi* is an especially physiologically and ecologically relevant taxon; it has an unusual wafer-thin (≤0.1 μm) square morphology, and it can withstand extreme desiccation, chaotropic stress, oxygen and nutrient limitation, and severe UV radiation (Bolhuis *et al*., 2006, 2017). This allows *H. walsbyi* to thrive in exceptionally inhospitable hypersaline brines where even other haloarchaea cannot.

The change in relative abundance of these major taxa with decreasing water activity reveals a continuous sequence of microbial succession in the transition from seawater to $MgCl_2$ brine (Fig. 4). The relative abundance of each major taxon in SBSW brines peaked at a different stage of evapoconcentration. *Halorubrum* peaked first (highest water activity) and began to decline around $a_w \approx 0.7$, followed closely by *Halohasta*. The next major taxon to peak was *Salinibacter*, around $a_w \approx 0.64$. *Haloquadratum* peaked last (lowest water activity), but rather than declining, its relative abundance appeared to plateau around 35%–40%. This plateau does not, however, imply that *Haloquadratum* continued to proliferate at water activities below 0.5 and $MgCl_2$ concentrations above 3 M. Rather, we hypothesize that 16S rRNA genes recovered from the $MgCl_2$ brines were remnants of the former, now-extinct microbial community, preserved by the chaotropic activity of the brines. Indeed, chaotropic salts have been shown to preserve extracellular DNA

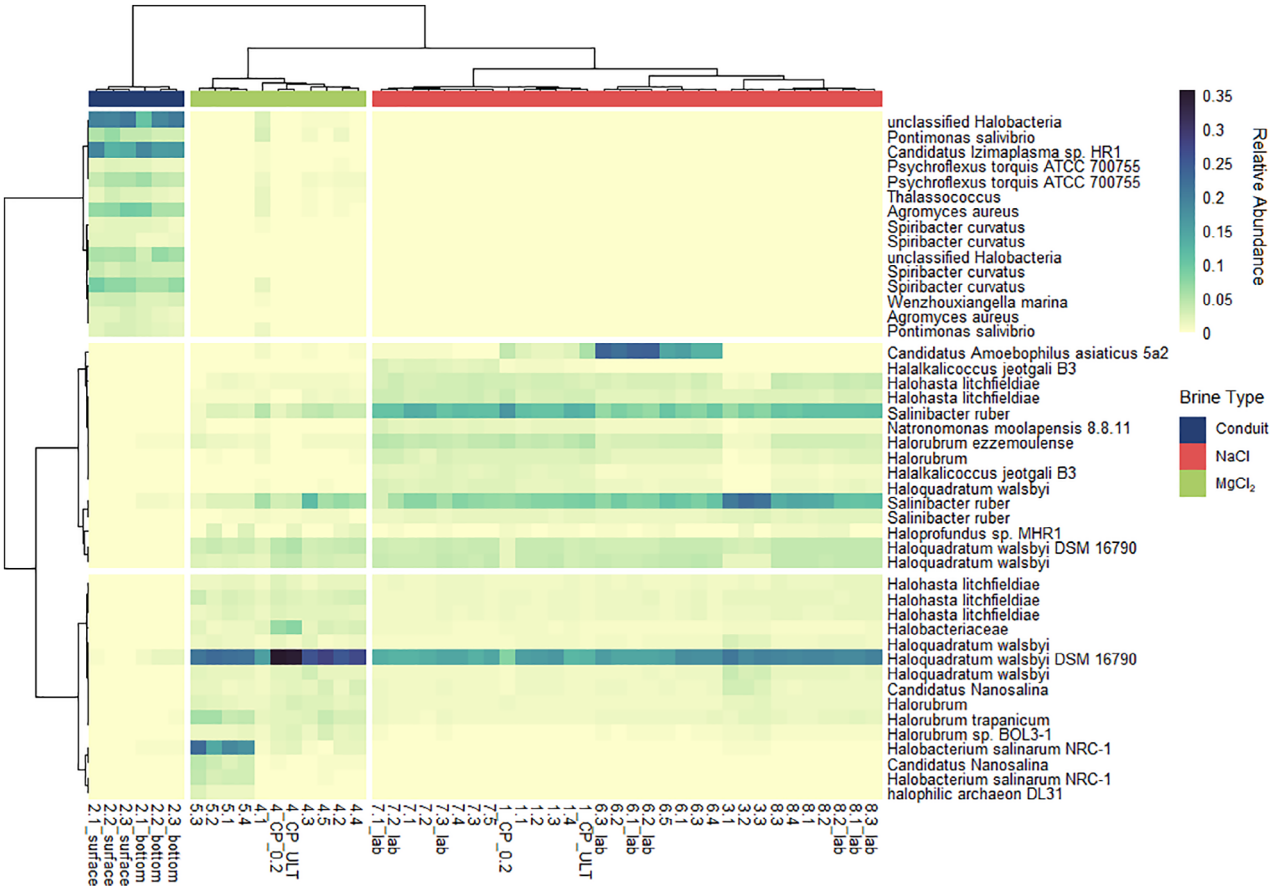


Fig 3. Community composition of SBSW brines. Heatmap shows relative abundance of common ASVs in each sample. Each row corresponds to a unique ASV, and row descriptions show the lowest consensus taxonomic classification for each ASV. Only ASVs that accounted for ≥2% of total reads (Illumina sequences) in at least one sample are shown. Hierarchical clustering of samples was based on the relative abundances of all ASVs, including those not shown above. Dendrograms show hierarchical clustering using Ward's minimum variance method, applied to (columns) Bray–Curtis dissimilarity between samples, and (rows) Spearman correlation between ASVs. [Color figure can be viewed at wileyonlinelibrary.com]

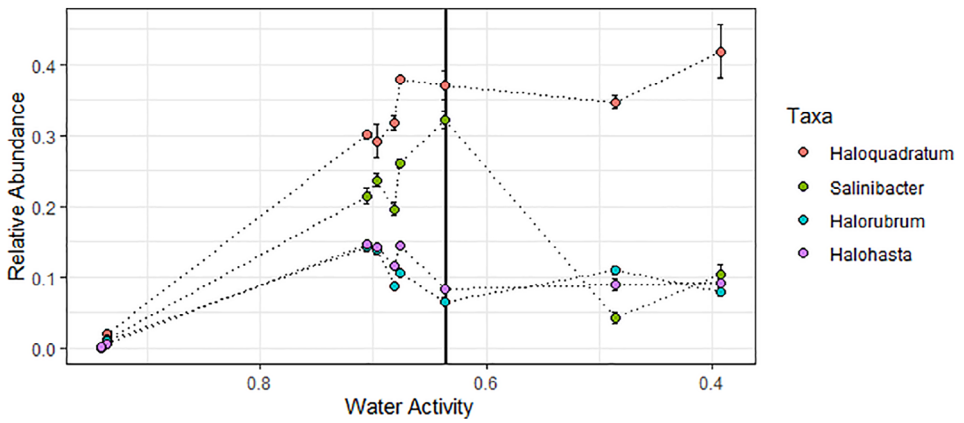


Fig 4. Changes in relative abundance of major taxa in SBSW brines with decreasing water activity. ASVs assigned to the same genus were aggregated and their relative abundances summed. Only genera that accounted for ≥10% of total reads (Illumina sequences) in two or more sites are shown. Points and error bars show (respectively) the mean and standard error of relative abundance between samples taken at the same site. The bold vertical line shows the known prokaryotic water activity limit of life (a_w = 0.635). [Color figure can be viewed at wileyonlinelibrary.com]

and rRNA for upwards of 45 days via the inhibition and denaturation of nucleases that would otherwise degrade free DNA (Duda *et al*., 2004; Hallsworth *et al*., 2007; Borin *et al*., 2008). Moreover, the extreme concentration of Mg^{2+} in these brines has the potential to further stabilize DNA by binding tightly to its negatively charged phosphate backbone and inducing stable packing conformations, thereby protecting DNA from degradation by abiotic and enzymatic processes (Luck and Zimmer, 1972; Chatake and Sunami, 2013; Serec *et al*., 2016).

Thus, the relative abundance of *Haloquadratum* (~35%–40%), *Salinibacter*, *Halorubrum* and *Halohasta* (~10% each) in the $MgCl_2$ brines is likely a preserved snapshot of the last active microbial community in the SBSW brines before they were rendered devoid of active life by desiccation and chaotropic stress (Oren, 2013). This interpretation supports previous research suggesting that *H. walsbyi* is the final survivor in thalassic hypersaline systems, capable of growth right up to the very limit of life in sublethal $MgCl_2$-rich, NaCl-saturated brines (Bolhuis *et al*., 2006, 2017).

Alpha and beta diversity

To identify patterns of archaeal and bacterial diversity along the water activity gradient, we estimated the ASV richness (Chao1) and phylogenetic diversity (Faith's PD) of each sample (Fig. 5). These results reveal several key processes occurring within the SBSW brines. The first is an explosion of archaeal richness in NaCl-saturated brines. ASV richness increased more than threefold from the conduit to the NaCl brines (ANOVA; $p = 0.005$). However, this increase in richness produced no significant increase in total phylogenetic diversity; archaeal phylogenetic diversity remained low and constant across the entire water activity gradient ($p = 0.216$). High ASV richness and low phylogenetic diversity indicate an abundance of very closely related ASVs (i.e. microdiversity). This surge in microdiversity was likely driven by rampant recombination among certain groups of haloarchaea, whose reputation for frequent horizontal gene transfer is well established (Boucher *et al*., 2004; Papke *et al*., 2004, 2015; Ram Mohan *et al*., 2014). Indeed, 77% of new ASVs in the NaCl brines were members of the class Halobacteria, and of these, *Haloquadratum*, *Halorubrum* and *Halohasta* alone accounted for 67%. Archaeal ASV richness peaked in the NaCl brines around $a_w \approx 0.7$, then tapered again as selection pressure further intensified with decreasing water activity and increasing chaotropicity.

It should be noted that ASV richness probably overestimates the actual diversity of unique organisms in these haloarchaea-dominated brines, since many haloarchaea (in particular *Haloarcula*) harbour multiple, divergent copies of the 16S rRNA gene (Boucher *et al*., 2004). Phylogenetic diversity, on the other hand, would not be affected by this intragenomic heterogeneity. When we corrected archaeal ASV richness for the number of unique 16S genes within the reference genome, the adjusted Chao1 estimates for the NaCl brines were ~40% lower than the original values. However, the overall patterns of alpha diversity (i.e. the explosion of archaeal microdiversity in NaCl-saturated brines) remained nearly unchanged.

Meanwhile, bacterial richness appeared to follow the exact opposite pattern: ASV richness was highest in the conduit and (somewhat surprisingly) in the presumably sterile $MgCl_2$ brines (ANOVA; $p = 0.003$). This V-shaped trend with decreasing water activity was even more pronounced when we considered the phylogenetic diversity of bacteria ($p < 0.001$). This remarkable increase of bacterial diversity, beginning within $0.68 \leq a_w \leq 0.64$ and continuing well beyond the chaotropicity and water activity limits of life, is further evidence of chaotropic preservation of DNA in bittern brines. However, rather than a snapshot of the last active microbial community, we hypothesize that the diverse bacterial 16S rRNA genes found in the $MgCl_2$-rich brines are infall: exogenous cells and genetic material that were introduced into the evaporation ponds from marine aerosols, bird faeces, rain, dust and other sources. Within NaCl brines, this infall is readily digested by living microbes and free nucleases. However, within the presumably sterile $MgCl_2$ brines, exogenous DNA is preserved by the extreme chaotropic activity, producing a surge in alpha diversity. Moreover, we expect that bacteria likely account for most of the infall (especially relative to the haloarchaea-dominated endogenous community) thereby causing a notable increase in bacterial diversity while producing no detectable signal in archaeal diversity.

Finally, in order to identify the primary axes of variation in microbial community composition between the various brines, we performed a Principal Coordinates Analysis (PCoA) based on Bray–Curtis dissimilarity between samples (Fig. 6A). PCoA Axis 1, which explains 58.4% of the total variation between samples, corresponds primarily to the change in microbial community composition between the conduit and the hypersaline brines, i.e. the proliferation of haloarchaea and *Salinibacter*. Axis 2, which explains 19.6% of the total variation, corresponds to the change in composition with decreasing water activity and increasing chaotropicity as the NaCl brines transitioned into $MgCl_2$ brines: an overall decrease in relative abundance of *Salinibacter*, *Halorubrum* and *Halohasta*, and ever-increasing *Haloquadratum*.

One notable result of this analysis is the relatively high Axis 1 values of the $MgCl_2$-saturated brines and $MgCl_2$-rich Site 3 samples ($a_w = 0.64$) compared with the rest of the NaCl brine samples (ANOVA; $p < 0.001$). This

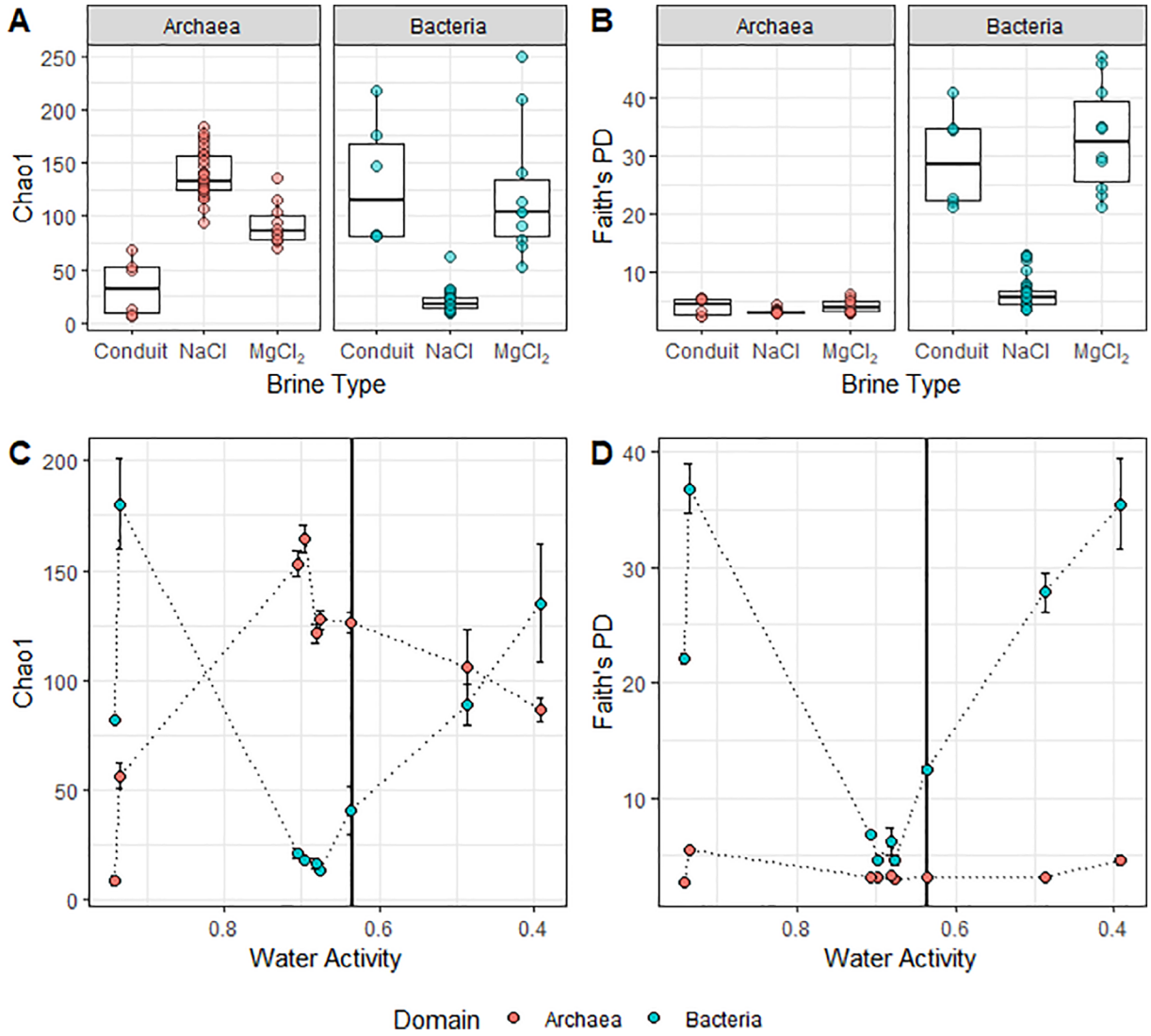


Fig 5. Changes in alpha diversity in SBSW brines with decreasing water activity.
A. Boxplots of estimated archaeal and bacterial ASV richness (Chao1) by brine type.
B. Boxplots of estimated archaeal and bacterial phylogenetic diversity (Faith's PD) by brine type.
C. Changes in Chao1 with decreasing water activity.
D. Changes in Faith's PD with decreasing water activity. In C and D, points and error bars show (respectively) the mean and standard error of diversity indices between samples taken at the same site. Bold vertical lines show the known prokaryotic water activity limit of life (a_w = 0.635). [Color figure can be viewed at wileyonlinelibrary.com]

suggests that the composition of the $MgCl_2$ brine communities lay between those of the conduit and NaCl brines (based on Bray–Curtis dissimilarity). Non-metric multidimensional scaling (NMDS) further supports this conclusion (Fig. 6B). Once again, this is likely the result of preserved infall; the community composition of the presumably sterile $MgCl_2$ brines started as a snapshot of the last active microbial community in the NaCl brines, but as exogenous cells and genetic material (consisting primarily of bacteria) began to accumulate, the composition gradually shifted towards that of the bacteria-dominated conduit. Indeed, Fig. 3 shows the overlap of certain taxa in the conduit and $MgCl_2$ brines, which were absent from the NaCl brines. Thus, infall rather than growth drives changes in 16S rRNA gene composition in these $MgCl_2$-rich brines. Moreover, since the conduit is most similar to seawater, we speculate that marine aerosols, in particular, contribute a significant portion of infall to the $MgCl_2$ brines.

Microbial activity and cell densities

To detect and quantify microbial activity in the various brines, samples from each site were incubated with ^{15}N-

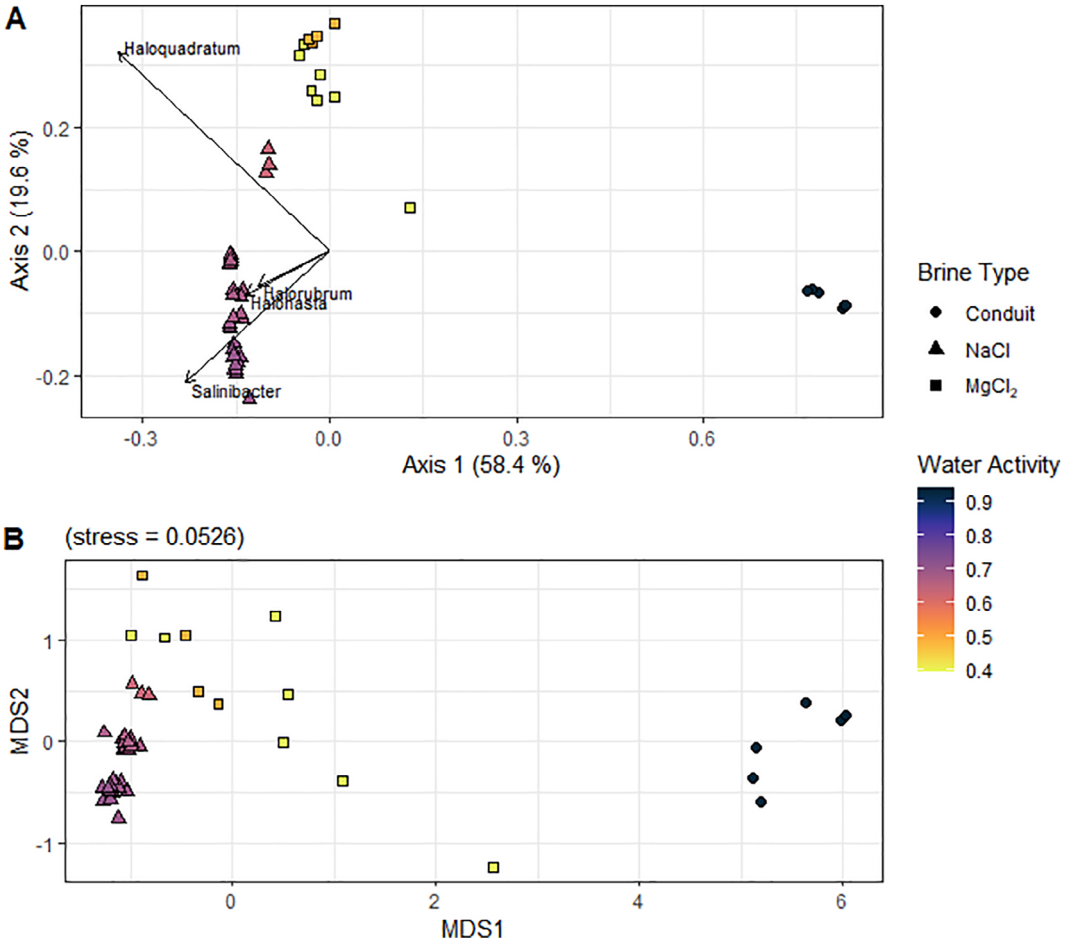


Fig 6. Ordination of changes in microbial community composition between SBSW brines. Ordinations based on Bray–Curtis dissimilarity between samples.
A. Principal Coordinates Analysis (PCoA). Relative eigenvalues with Lingoes correction are shown in parentheses. Response variables (relative abundance of major taxa) were projected *a posteriori* onto the PCoA axes (as in PCA) without scaling.
B. Non-metric multidimensional scaling (NMDS). Stress value is shown in parentheses. [Color figure can be viewed at wileyonlinelibrary.com]

ammonium. We also incubated a 50% dilution of the brine from Site 4 with ^{15}N-ammonium, as we hypothesized that increasing water activity and reducing ionic strength would increase microbial activity (final a_w = 0.812). Uptake of ^{15}N-ammonium has been used as a proxy for microbial anabolic activity in diverse environments (e.g., Krüger *et al*., 2008; Dawson *et al*., 2016), with the assumption that the vast majority of microorganisms are able to assimilate it. Genes related to ammonium uptake and assimilation (e.g. ammonium transporter, glutamine synthetase, glutamate synthase) have been identified in many halophiles, including *H. walsbyi* and *S. ruber* (Mongodin *et al*., 2005; Bolhuis *et al*., 2006), and ammonium incorporation has been directly observed in the model haloarchaeon, *Haloferax mediterranei* (Bonete *et al*., 2008), suggesting it can be readily assimilated by the community members at SBSW. DNA analysis of samples taken before, during and after the incubation showed that no major changes in microbial community composition occurred as a result of the incubation (see Supplementary Fig. S1 for details).

After 48 h, the ^{15}N/^{14}N ratio of individual cells was measured by nanoSIMS (Fig. 7). We chose single-cell measurements rather than bulk measurements (e.g. via isotope ratio mass spectrometry) in order to maximize the potential to detect low levels of activity within even rare active cells. The limit of detection for ^{15}N-assimilation was determined for each site using the mean and standard deviation of the ^{15}N/^{14}N ratio in cells fixed at t_0 (i.e. prior to ^{15}N-ammonium incubation), resulting in single-cell ammonium-based growth rate detection limits ranging from 0.003 to 0.007 day^{-1} (see Supplementary Table S5 for site-specific detection limits). Despite this low threshold, activity was detected only in the conduit samples, where 18.0% of cells from the surface (n = 61) and 9.5% of cells from the bottom (n = 95) were enriched

after 48 h. No cells from the NaCl or $MgCl_2$ brines assimilated detectable amounts of ^{15}N-ammonium. This result was unexpected, given that water activity in the Site 1 incubations (a_w = 0.720) was within the habitable window for haloarchaea ($a_w \geq 0.635$) and suggests either higher sensitivity to desiccation than previously characterized lineages or the role of additional parameters limiting microbial growth. These results suggest an upper bound for metabolic activity within the hypersaline brines under our incubation conditions ($\leq$0.003 day^{-1}). For comparison, when grown on optimal media near room temperature, cultured representatives of the class Halobacteria have specific growth rates on the order of 1 day^{-1} (Robinson *et al*., 2005). Though the environmental conditions at SBSW might be better suited for haloarchaea to grow, the extremely low rates of metabolic activity in the experimental incubations suggest low *in situ* growth rates within the SBSW hypersaline brines as well.

In addition to activity, we estimated cell densities in each of the brines using both flow cytometry and microscope counts. Diverse cell morphologies were observed within all of the sites (Supplementary Fig. S2). We found that cell densities were quite high in the NaCl brines using both methods (~10^7 cells ml^{-1}; see Supplementary Table S6 for detailed cell density estimates). When considered alongside the extremely low rates of microbial activity, the high cell densities in the NaCl brines suggest that rates of grazing and viral mortality are very low in this system. Thus, biomass is allowed to accumulate. From an astrobiological perspective, this means that organic molecules (i.e. potential biomarkers) can become highly concentrated (and therefore, may be easier to detect) in hypersaline brines despite the extreme nature of the environment. However, even in very high biomass environments, cellular activity may be difficult to detect.

Both flow cytometry and microscope counts indicated that cells were present in the $MgCl_2$ brines, though at much lower densities (10^4–10^5 cells ml^{-1}). We hypothesize that these were 'fossil' (non-viable, preserved) cells, as the $MgCl_2$ brines were presumably sterile. Indeed, previous research has shown that most cells are lysed by the extreme physiological stress exerted on membranes and other cellular structures in chaotropic brines (Duda *et al*., 2004; Borin *et al*., 2008). However, some microbes and spores with particularly tough cell walls (e.g. yeasts, mycelial fungi and Gram-positive bacteria) are not completely degraded and retain their shape as cell sheaths containing loose bundles of DNA and remnants of the cytoplasm, known as micromummies (Duda *et al*., 2004). Our hypothesis that the cell-like structures in the $MgCl_2$ brines were in fact preserved micromummies rather than viable cells was further supported by the results of the dilution-nanoSIMS experiment; increasing the water activity via dilution did not stimulate growth within the Site 4 brines (Fig. 7).

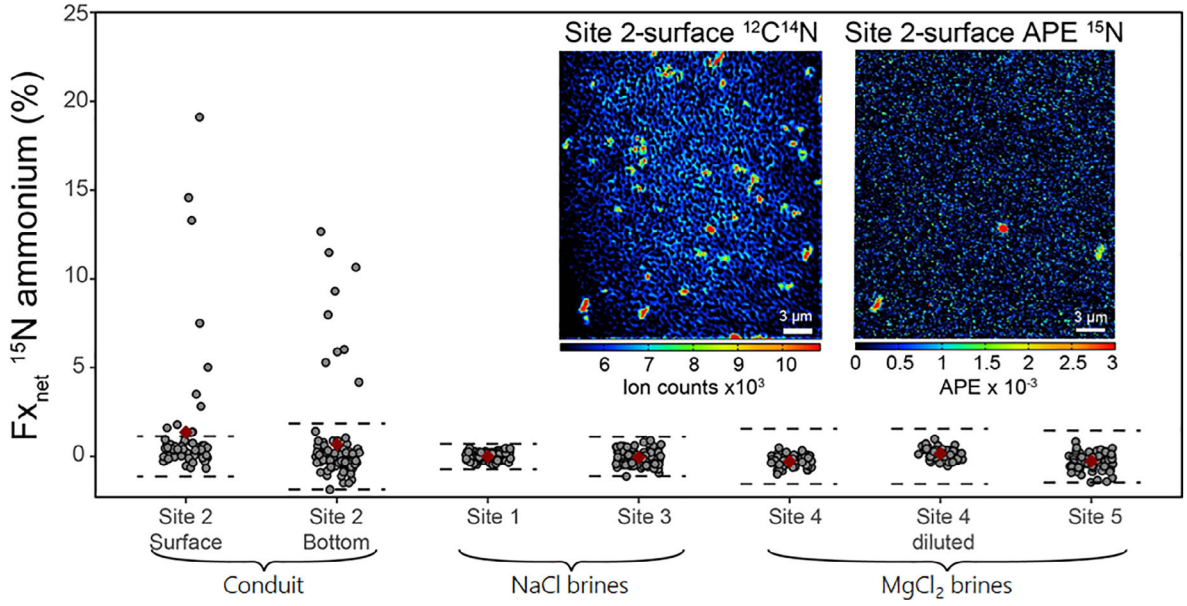


Fig 7. NanoSIMS analysis of ^{15}N-ammonium incorporation in individual cells from each site. The scatter plot shows the net fixation rates of ^{15}N for each site. The red dot indicates the average Fx_{net} value, and the black dashed lines represent site-specific detection limits (see Experimental procedures). The insets show nanoSIMS images of cells from Site 2-surface, specifically $^{12}C^{14}N^-$ ion counts and corresponding ^{15}N atom percent excess (APE), showing few cells enriched in ^{15}N. [Color figure can be viewed at wileyonlinelibrary.com]

© 2021 Society for Applied Microbiology and John Wiley & Sons Ltd.,

Conclusions and broader significance

Together, our various analyses reveal a coherent picture of the changes in microbial diversity and composition with seawater evaporation in the SBSW brines, which we believe may be representative of thalassic evaporative systems in general. The observed changes occurred in three distinct stages, spanning the wide range of water activity and chaotropicity present within the various SBSW brines. We estimated the a_w ranges within which each of these stages occur, to the extent possible given the distribution of our observations along the water activity gradient. Future work to fill in this entire gradient (in particular, $0.93 \leq a_w \leq 0.70$) is desirable to specify precise a_w thresholds with greater certainty.

The first stage ($1 \leq a_w \leq 0.7$) was characterized by microbial growth and adaptation to increasingly severe desiccation, along with a multitude of other environmental stresses. In this stage, we observed an explosion of haloarchaeal abundance and microdiversity. This allowed haloarchaea to adapt to and colonize the increasingly restrictive ecological niches in these hypersaline brines, while the majority of other archaea and bacteria (except for halophilic bacterium *Salinibacter ruber*) crashed out of the microbial community. The second stage ($0.7 \leq a_w \leq 0.64$) was characterized by progressively more intense selection pressure due to increasing chaotropicity and ever-decreasing water activity. Brines in this stage were increasingly dominated by *H. walsbyi* and *S. ruber*, as the conditions become too inhospitable even for most haloarchaea, which began to die off one by one. Eventually, even *S. ruber* could no longer survive the extreme osmotic and chaotropic stress, leaving *H. walsbyi* alone to dominate the now-$MgCl_2$-rich brines. Finally, at some point, the water activity/chaotropicity limit of life was surpassed, rendering the remaining brine metabolically inactive. This third and final stage ($a_w < 0.64$) was characterized by a 'fossil' microbial community consisting of chaotropically preserved extracellular DNA and cell remnants known as micromummies. In the absence of active microbial life, this fossil community began as a snapshot of the last active community (i.e. primarily just *H. walsbyi*), but as cells and bits of genetic material fall into the brine and get preserved, it gradually accumulated a diverse assemblage of 16S rRNA genes.

This remarkable increase in 16S rRNA gene diversity (particularly bacterial diversity) allowed us to estimate the water activity/chaotropicity limit of life in the SBSW brines. We assume that the flux of infall into hypersaline brines is constant across the entire process of evapoconcentration, and small relative to the endogenous microbial community. Furthermore, extracellular genetic material is short-lived in brines with active microbial communities, due to digestion by living microbes and free nucleases. Thus, infall does not produce a detectable alpha diversity signal until the limit of life is exceeded, free nucleases are denatured and preserved exogenous 16S rRNA genes can begin to accumulate. We, therefore, hypothesize that the preservation of exogenous genetic material is a major difference between habitable NaCl brines and highly chaotropic, presumably sterile $MgCl_2$ brines. In the SBSW system, this marked increase in diversity began somewhere in the range of $0.68 \leq a_w \leq 0.64$. Our results do not offer a conclusive indication of whether the water activity or chaotropicity limit of life was exceeded first, but studies of other $MgCl_2$-rich hypersaline systems have suggested that chaotropicity constrains the habitable window (Hallsworth *et al*., 2007). Moreover, our approximation for the limit of life in the SBSW brines ($0.68 \leq a_w \leq 0.64$) is slightly higher than the known prokaryotic water activity limit ($a_w = 0.635$), allowing us to speculate that chaotropicity is more restrictive in this environment. In any case, osmotic and chaotropic stress in this system are concomitant and highly correlated.

The results of this study have implications for the search for extraterrestrial life relevant to future life-detection missions. Constraining the limits of life in terrestrial hypersaline systems will help guide our search for habitable worlds, from the ancient remnant oceans of Mars to the briny oceans of Europa and Enceladus. Refining our understanding of how chaotropicity and water activity interact to define the habitable window is therefore a priority for future research. Furthermore, our conclusion that 16S rRNA genes were preserved in the presumably sterile $MgCl_2$ brines at SBSW supports previous research showing that chaotropic activity conserves DNA (Duda *et al*., 2004; Hallsworth *et al*., 2007; Borin *et al*., 2008). Thus, DNA is a poor biomarker for extant life in chaotropic brines. However, it is potentially an excellent biomarker for *extinct* life in these environments, since survivability is an essential criterion for life detection (Neveu *et al*., 2018). Life on other worlds may utilize nucleic acids under conditions of shared ancestry with terrestrial life or common physiochemistry; more broadly, it has been argued that long, charged informational polymers may be universal for aqueous-based life (Benner, 2017). Moreover, our finding that exogenous genetic material is preserved in $MgCl_2$-rich brines suggests that chaotropic brines could serve as repositories for genetic biomarkers of life in nearby environments. This, along with the potential for accumulating cell micromummies and high concentrations of organic molecules, makes hypersaline brines in general, and chaotropic brines in particular, worthwhile targets in the search for extraterrestrial life.

Experimental procedures

Sampling and in situ *geochemical measurements*

Samples were collected over the course of a 2-day fieldtrip to SBSW on August 6–7, 2019. Geochemical parameters were measured *in situ* at each site (Fig. 1) with an AQUALAB 4TE dew point water activity meter (a_w) and a Hanna HI98194 multiparameter meter (temperature, pH, conductivity, redox). See Supplementary Table S1 for complete *in situ* measurements. For DNA analysis, a small volume of brine (300–400 ml for conduit samples; 3–10 ml for hypersaline brines due to extreme viscosity) was filtered through a sterile 47 mm, 0.2 μm Supor filter (PALL) directly from each site using a peristaltic pump. Filters were kept on dry ice until they could be returned to the lab, where they were stored at −80°C for later DNA purification. Samples were collected from both the surface and near the bottom of the conduit (Site 2), and from approximately the middle of the shallow water column (∼30 cm) in the evaporation ponds (Sites 1 and 3–8).

Brine samples for ion measurements, nanoSIMS analysis, microscopy and flow cytometry were collected in acid-washed PP or LDPE bottles using a peristaltic pump and stored at room temperature to prevent salt crystallization until they could be returned to the lab (within 6 h). Back at the lab (in order to ensure that our sampling methods did not significantly alter the microbial community composition) we filtered 1 ml of brine from Sites 6 to 8 through 25 mm, 0.2 μm Supor filters (PALL) for further DNA analysis. Filters were stored at −80°C for later DNA purification. These samples are denoted with the suffix '_lab'. In addition, brines from Sites 1 and 4 were prefiltered through 330 μm mesh filters (HC08016) and concentrated with an InnovaPrep CP Select concentrating pipette (InnovaPrep) using the PS 0.2 μm (CC08022) and ultrafilter (CC08003) tips. These samples are denoted with the suffix '_CP_0.2' and '_CP_ULT' respectively. Samples were eluted with a wet CO_2 foam (InnovaPrep HC08001, 0.075% Tween 20/Tris) in ∼300 μl and stored at −80°C for later DNA purification.

Dissolved ion concentrations

Brine samples were sent to ACZ Laboratories (Steamboat Springs, Colorado) for determination of dissolved metals and sulfur concentrations (Al, B, Ca, Co, Fe, Mg, Mn, Mo, Ni, K, Se, Si, Na, S, Zn) and inorganic anions (Br^-, Cl^-, Fl^-, SO_4^{2-}). Metals and sulfur were measured using inductively coupled plasma atomic emission spectrometry (Martin *et al*., 1994). Anions were measured using ion chromatography (Pfaff, 1993). See Supplementary Tables S2 and S3 for complete results. For comparison with other studies of $MgCl_2$-rich brines, the concentration of $MgCl_2$ was estimated to be either ($[Mg^{2+}] - [SO_4^{2-}]$) or ($[Cl^-] - [Na^+]$) ÷ 2, whichever was smaller.

Seawater evaporation model

The evaporation of seawater was simulated computationally using EQ3/6 (Wolery and Jarek, 2003). EQ3/6 is a family of codes composed of a speciation-solubility code (EQ3NR) and a reaction-path code (EQ6). The thermodynamic databases used are hmw (derived after the equations of Harvie *et al*., 1984) for the speciation-solubility model and ypf (yucca mountain project pitzer datafile) for the reaction-path evaporation model. Both use the Pitzer equations to calculate activity coefficients. This step was necessary due to the high ionic strength of brines. The hmw database is limited to 25°C, whereas the ypf database allows for a broader range of temperatures. We first equilibrated generic seawater (Nordstrom *et al*., 1979) at 25°C, electrically balanced with Cl^-, using EQ3. We then used EQ6 to evaporate the resulting seawater on a sliding temperature scale from T_{init} = 25°C (Site 2) to T_{final} = 40°C (Site 4).

The code computes the activity of chemical species at thermodynamic equilibrium. In contrast, seawater is supersaturated with respect to calcium carbonate. Given the thermodynamic equilibrium nature of EQ3/6, supersaturation is not allowed and the equilibrium code precipitates out excess carbonate as a solid mineral. This reaction is a source of H^+, and thus acidifies the numerical equilibrium fluid via the following equation:

$$Ca^{2+} + HCO_3^- \rightarrow CaCO_3(s) + H^+$$

To correct for the effect of supersaturation within the constraints of an equilibrium code, pH values were shifted up by 0.79 to account for the differences between the measured pH of supersaturated seawater (8.22) and that predicted at thermodynamic equilibrium (7.43 at 25°C). The pH-corrected results are illustrated in Fig. 2. The EQ6 evaporation input file is included in the Supplementary Material.

DNA purification and sequencing

DNA was extracted from filters using the MagMax Microbiome Ultra Nucleic Acid Isolation Kit (Fisher) and KingFisher Flex (ThermoFisher). A quarter of each 47 mm filter or whole 25 mm filters were used for extraction. DNA concentrations were measured using Qubit dsDNA high-sensitivity assay (Invitrogen; see Supplementary Table S4). Purified DNA was then sent to Argonne National Laboratory for 16S rRNA gene amplification,

library preparation and sequencing. 515F/806R universal prokaryotic primers were used for 16S rRNA gene amplification (Walters *et al*., 2015). Amplicon libraries were 2 × 151 paired-end sequenced on the Illumina MiSeq platform. Illumina reads and accompanying metadata were uploaded to the NCBI Sequence Read Archive (SRA) under BioProject PRJNA680352.

Sequence treatment and analysis

Paired-end Illumina reads were quality-filtered, denoised and merged using the DADA2 pipeline (R-package 'dada2' v1.14) (Callahan *et al*., 2016). The merged reads (fasta files) were then used as an input for the paprica pipeline for microbial community structure and metabolic inference (paprica v0.5) (Bowman and Ducklow, 2015). With paprica, 16S sequence variants were first aligned using Infernal (Nawrocki and Eddy, 2013), and then placed using pplacer (Matsen *et al*., 2010) on a reference tree constructed from all completed prokaryotic genomes available in the RefSeq database (Haft *et al*., 2018), and assigned to taxonomic groups based on their phylogenetic placement. Abundant, ambiguous ASVs that could not be classified with paprica were assigned taxonomic data using the web-based RDP Classifier tool (https://rdp.cme.msu.edu/classifier). The outputs of paprica - phylogenetic placements (jplace files) and ASV abundance matrices normalized by estimated 16S gene copy number - were used for downstream diversity analyses. Bray–Curtis dissimilarities, ANOSIM and NMDS were computed using R-package 'vegan' v2.5–6 (Oksanen *et al*., 2019). In order to estimate alpha diversity indices (Chao1 and Faith's PD), 16S reads were first subsampled (n = 12 500) in order to normalize for variation in sequencing depth between samples. Sample '5.3' was excluded due to the low number of total reads (n = 4008). Phylogenetic diversity (Faith's PD) was calculated using guppy, a program included with pplacer. Finally, PCoA ordination was performed using R-package 'ape' v5.3 (Paradis and Schliep, 2019).

Stable isotope incubations

Brine samples from each site were prefiltered through 330 μm mesh (HC08016) to exclude metazoans and large debris. 200 ml of prefiltered brine was distributed into duplicate 250 ml polycarbonate bottles for incubation experiments. A 50% dilution of brine from Site 4 was prepared with deionized water. Water activity measured within the incubations was slightly higher than that measured in the field due to precipitation of some salts during incubation setup: Site 1, a_w = 0.720; Site 2, a_w = 0.935; Site 3, a_w = 0.668; Site 4, a_w = 0.435; Site 5, a_w = 0.517. Isotopically labelled ammonium chloride ($^{15}NH_4Cl$, ^{15}N 99%, Cambridge Laboratories), sodium bicarbonate ($NaH^{13}CO_3$, ^{13}C 99%, Cambridge Laboratories) and deuterated water (D_2O, D 99.8%, Cambridge Laboratories) were added to each bottle for final concentrations of 200 nM $^{15}NH_4Cl$, 200 μM $NaH^{13}CO_3$ and 10% D_2O by volume. Due to higher detection limits for ^{13}C and D incorporation relative to ^{15}N, and the absence of detectable ^{13}C or D incorporation in any cells, these isotopes were not considered in further analyses (See Supplementary Table S5). Bottles were incubated for 48 h at room temperature (~25°C) with a 12-h:12-h light/dark photoperiod using a red-blue artificial light source. At the end of each incubation, a small aliquot of brine was filtered through a 0.22 μm-pore-diameter filter (Sterivex) for 16S amplicon sequencing and DNA analysis (see DNA purification and sequencing methods above).

NanoSIMS analysis

At the end of the 48-h incubation period, 50 ml of brine from each bottle was fixed with 4% formaldehyde for 3 h at room temperature. 1 ml of each sample was filtered through 0.2 μm-pore-diameter polycarbonate filters (Millipore) using a Millipore multi-position vacuum filtration system. Filters were washed with PBS and 70% ethanol, air-dried for 10–15 min and frozen. Filter pieces were mounted on adhesive carbon holders and sputter coated with *c*. 20 nm of gold. Prepared samples were then analysed with a CAMECA NanoSIMS 50 L (Cameca, Gennevilliers, France) housed within the Stanford NanoFacility at Stanford University. A ~5 pA Cs^+ primary beam was used in a 256 × 256-pixel raster. Dwell time was ~1 ms/pixel, and raster size was 30 μm^2. Seven secondary ions were detected in simultaneous collection mode ($^{12}CH^-$, $^{12}CD^-$, $^{12}C_2^-$, $^{12}C^{13}C^-$, $^{12}C^{14}N^-$, $^{12}C^{15}N^-$ and $^{31}P^-$) producing 45 serial secondary ion images (analysis layers). The mass spectrometer was tuned for ~8000 mass resolving power to resolve isobaric interferences. Samples were pre-sputtered for 30 s to partially remove the gold covering the cells. A minimum of 50 cells were analysed for each sample at both t = 0 and t = 48-h time points. Fixed *Sulfolobus* cells of known isotopic composition were used as standards.

Quantification of isotope assimilation and growth rates

The nanoSIMS data were analysed using LANS software (Polerecky *et al*., 2012) allowing for the accumulation of the scans with lateral drift correction and quantitative analysis of isotopic ratios ($^{12}C^{15}N^-/^{12}C^{14}N^-$). To determine cell-specific isotope ratios, regions of interests (ROIs) were drawn inside the cells, avoiding the cell-surrounding areas. ROIs were drawn using the $^{12}C^{14}N^-$ channel. To calculate the net ^{15}N assimilation rates

relative to the initial biomass we used the equation proposed by Popa *et al*. (2007) and Pett-Ridge and Weber (in press):

$$Fx_{net} = \frac{\left\{R_f\left[1-\frac{R_i}{R_i+1}\right]-\frac{R_i}{R_i+1}\right\}}{\left\{\frac{R_s}{R_s+1}-R_f\left[1-\frac{R_s}{R_s+1}\right]\right\}} \times 100\%$$

where R_i is the initial isotope ratio of the organism (at t_0), R_f is the final isotope ratio of the organism (calculated here after 48 h of incubation) and R_s is the isotope ratio of the substrate pool (e.g. in the case of ammonium, $R_s = 0.04$, as we added 4% of ^{15}N-ammonium). Cells were considered active if R_f exceeded three times the standard deviation (3SD) over the mean R_i for a given site, as described in Dekas *et al*. (2019). In addition - to conservatively account for potential variation in precision between the t_0 and 48-h samples due to differences in ion yield - if the R_f of any cell was more than 3SD below the mean R_i for that site, $|R_f - R_i|$ for the cell with the lowest R_f was used as the detection limit for that particular site (Site 2-bottom, Site 3 and Site 5). Isotope-specific growth rates to determine detection limits for each site were calculated according to the following equation:

$$\mu_{cells} = \frac{\ln(1+K_A)}{t_1 - t_0}$$

K_A is the fraction of the isotope incorporated by the cell relative to the initial isotope content calculated according to Stryhanyuk *et al*. (2018):

$$K_A = \frac{R_f - R_i}{(1+R_i)\times[R_s\times(1+R_f)-R_f]}$$

Cell density estimation

To determine microbial abundance in each site (Supplementary Table S6), fixed cells from each of the brines and the conduit were collected onto 0.2 μm polycarbonate filters (Millipore) and stained with 4′,6-diamidino-4-phenylindole (1 μg ml^{-1}, 30 min). Microbial abundance was analysed by acquiring images using an epifluorescence microscope equipped with a digital camera (Leica). Cell abundance was quantified by ACMEtool2 (Zeder *et al*., 2010) and CellC (Selinummi *et al*., 2005) image analysis software, and spot checked manually.

Cell abundance was also quantified by flow cytometry following the methods of Webb *et al*. (2019). In brief, samples were fixed to 4% formaldehyde and diluted 10:1 with a 4% PBS solution. Samples for the analysis of non-autofluorescent cells were stained with SYBR Green I (Molecular Probes) following the manufacturer's instructions. Samples were spiked with a known concentration of 123count eBeads (Thermo-Fisher) and run on a CyFlow Space flow cytometer (Sysmex). Flow cytometry data were analysed in R using the flowCore library (Ellis *et al*., 2020) and custom scripts (https://github.com/bowmanlab/flow_cytometry_scripts).

Acknowledgements

This work was part of the Oceans Across Space and Time (OAST) project, funded by NASA's Astrobiology Program award 80NSSC18K1301 (PI: B.E. Schmidt). We are grateful to the entire OAST team for their support and expertise. We also thank the South Bay Salt Works and Brian Collins at the San Diego Bay National Wildlife Refuge for facilitating this effort. We wish to acknowledge Andrew Mueller (UC San Diego) for his support in the lab. Finally, we thank Téa Cohen and Christie Jilly-Rehak (Stanford University) for assistance with microscope cell counts and nanoSIMS measurements respectively. NanoSIMS measurements were performed at the Stanford Nano Shared Facility (SNSF), which is supported by the National Science Foundation under award ECCS-1542152.

References

Altheide, T., Chevrier, V., Nicholson, C., and Denson, J. (2009) Experimental investigation of the stability and evaporation of sulfate and chloride brines on Mars. *Earth Planet Sci Lett* **282**: 69–78.

Antón, J., Oren, A., Benlloch, S., Rodríguez-Valera, F., Amann, R., and Rosselló-Mora, R. (2002) *Salinibacter ruber* gen. nov., sp. nov., a novel, extremely halophilic member of the bacteria from saltern crystallizer ponds. *Int J Syst Evol Microbiol* **52**: 485–491.

Ball, P., and Hallsworth, J.E. (2015) Water structure and chaotropicity: their uses, abuses and biological implications. *Phys Chem Chem Phys* **17**: 8297–8305.

Benner, S.A. (2017) Detecting Darwinism from molecules in the Enceladus plumes, Jupiter's moons, and other planetary water lagoons. *Astrobiology* **17**: 840–851.

Bolhuis, H., Martín-Cuadrado, A.B., Rosselli, R., Pašić, L., and Rodriguez-Valera, F. (2017) Transcriptome analysis of *Haloquadratum walsbyi*: vanity is but the surface. *BMC Genomics* **18**: 510.

Bolhuis, H., Palm, P., Wende, A., Falb, M., Rampp, M., Rodriguez-Valera, F., *et al*. (2006) The genome of the square archaeon *Haloquadratum walsbyi*: life at the limits of water activity. *BMC Genomics* **7**: 169.

Bonete, M.J., Martínez-Espinosa, R.M., Pire, C., Zafrilla, B., and Richardson, D.J. (2008) Nitrogen metabolism in haloarchaea. *Saline Syst* **4**: 9.

Borin, S., Crotti, E., Mapelli, F., Tamagnini, I., Corselli, C., and Daffonchio, D. (2008) DNA is preserved and maintains transforming potential after contact with brines of the deep anoxic hypersaline lakes of the eastern Mediterranean Sea. *Saline Syst* **4**: 10.

Boucher, Y., Douady, C.J., Sharma, A.K., Kamekura, M., and Doolittle, W.F. (2004) Intragenomic heterogeneity and intergenomic recombination among haloarchaeal rRNA genes. *J Bacteriol* **186**: 3980–3990.

Bowman, J.S., and Ducklow, H.W. (2015) Microbial communities can be described by metabolic structure: a general framework and application to a seasonally variable, depth-stratified microbial community from the coastal West Antarctic Peninsula. *PLoS One* **10**: e013586.

Callahan, B.J., Mcmurdie, P.J., Rosen, M.J., Han, A.W., Johnson, A.J.A., and Holmes, S.P. (2016) DADA2: high-resolution sample inference from Illumina amplicon data. *Nat Methods* **13**: 581–583.

Chatake, T., and Sunami, T. (2013) Direct interactions between Z-DNA and alkaline earth cations, discovered in the presence of high concentrations of $MgCl_2$ and $CaCl_2$. *J Inorg Biochem* **124**: 15–25.

Cray, J.A., Russell, J.T., Timson, D.J., Singhal, R.S., and Hallsworth, J.E. (2013) A universal measure of chaotropicity and kosmotropicity. *Environ Microbiol* **15**: 287–296.

Cubillos, C.F., Paredes, A., Yáñez, C., Palma, J., Severino, E., Vejar, D., *et al*. (2019) Insights into the microbiology of the chaotropic brines of Salar de Atacama, Chile. *Front Microbiol* **10**: 1611.

Dawson, K.S., Scheller, S., Dillon, J.G., and Orphan, V.J. (2016) Stable isotope phenotyping via cluster analysis of nanoSIMS data as a method for characterizing distinct microbial ecophysiologies and sulfur-cycling in the environment. *Frontiers in Microbiology* **7**: 774.

Dekas, A.E., Parada, A.E., Mayali, X., Fuhrman, J.A., Wollard, J., Weber, P.K., and Pett-Ridge, J. (2019) Characterizing chemoautotrophy and heterotrophy in marine archaea and bacteria with single-cell multi-isotope nanoSIP. *Front Microbiol* **10**: 2682.

Duda, V.I., Danilevich, V.N., Suzina, N.E., Shorokhova, A.P., Dmitriev, V.V., Mokhova, O.N., and Akimov, V.N. (2004) Changes in the fine structure of microbial cells induced by chaotropic salts. *Microbiology* **73**: 341–349.

Ellis, B., Haaland, P., Hahne, F., Le Meur, N., Gopalakrishnan, N., Spidlen, J., *et al*. (2020) flowCore: Basic structures for flow cytometry data. R package version 2.0.1.

Fernández-Remolar, D.C., Chong-Díaz, G., Ruíz-Bermejo, M., Harir, M., Schmitt-Kopplin, P., Tziotis, D., *et al*. (2013) Molecular preservation in halite- and perchlorate-rich hypersaline subsurface deposits in the Salar Grande basin (Atacama Desert, Chile): implications for the search for molecular biomarkers on Mars. *J Geophys Res Biogeosci* **118**: 922–939.

Fredrickson, J.K., Chandler, D.P., and Onstott, T.C. (1997) Potential for preservation of halobacteria and their macromolecular constituents in brine inclusions from bedded salt deposits. *Proc SPIE* **3111**: 318–329.

Haft, D.H., DiCuccio, M., Badretdin, A., Brover, V., Chetvernin, V., O'Neill, K., *et al*. (2018) RefSeq: an update on prokaryotic genome annotation and curation. *Nucleic Acids Res* **46**: D851–D860.

Hallsworth, J.E., Yakimov, M.M., Golyshin, P.N., Gillion, J.L. M., D'Auria, G., De Lima Alves, F., *et al*. (2007) Limits of life in $MgCl_2$-containing environments: chaotropicity defines the window. *Environ Microbiol* **9**: 801–813.

Harvie, C.E., Møller, N., and Weare, J.H. (1984) The prediction of mineral solubilities in natural waters: the Na-K-Mg-Ca-H-Cl-SO_4-OH-HCO_3-CO_3-CO_2-H_2O system to high ionic strengths at 25°C. *Geochim Cosmochim Acta* **48**: 723–751.

Krüger, M., Wolters, H., Gehre, M., Joye, S.B., and Richnow, H.H. (2008) Tracing the slow growth of anaerobic methane-oxidizing communities by ^{15}N-labelling techniques. *FEMS Microbiol Ecol* **63**: 401–411.

Luck, G., and Zimmer, C. (1972) Conformational aspects and reactivity of DNA: effects of manganese and magnesium ions on interaction with DNA. *Eur J Biochem* **29**: 528–536.

Martin, T.D., Brockhoff, C.A., Creed, J.T., and EMMC Methods Work Group. (1994) *Method 200.7: Determination of Metals and Trace Elements in Water and Wastes by Inductively Coupled Plasma-Atomic Emission Spectrometry*. Revision 4.4, Cincinnati, OH: US EPA.

Matsen, F.A., Kodner, R.B., and Armbrust, E.V. (2010) pplacer: linear time maximum-likelihood and Bayesian phylogenetic placement of sequences onto a fixed reference tree. *BMC Bioinformatics* **11**: 538.

Mongodin, E.F., Nelson, K.E., Daugherty, S., Deboy, R.T., Wister, J., Khouri, H., *et al*. (2005) The genome of *Salinibacter ruber*: convergence and gene exchange among hyperhalophilic bacteria and. *Archaea* **102**: 18147–18152.

Narasingarao, P., Podell, S., Ugalde, J.A., Brochier-Armanet, C., Emerson, J.B., Brocks, J.J., *et al*. (2012) De novo metagenomic assembly reveals abundant novel major lineage of archaea in hypersaline microbial communities. *ISME J* **6**: 81–93.

Nawrocki, E.P., and Eddy, S.R. (2013) Infernal 1.1: 100-fold faster RNA homology searches. *Bioinformatics* **29**: 2933–2935.

Nazari-Sharabian, M., Aghababaei, M., Karakouzian, M., and Karami, M. (2020) Water on Mars—a literature review. *Galaxies* **8**: 40.

Neveu, M., Hays, L.E., Voytek, M.A., New, M.H., and Schulte, M.D. (2018) The ladder of life detection. *Astrobiology* **18**: 1375–1402.

Nordstrom, D.K., Plummer, L.N., Wigley, T.M.L., Wolery, T. J., Ball, J.W., Jenne, E.A., *et al*. (1979) A comparison of computerized chemical models for equilibrium calculations in aqueous systems. In *Chemical Modeling in Aqueous Systems*, Jenne, E.A. (ed). Washington, DC: American Chemical Society, pp. 857–892.

Oh, D., Porter, K., Russ, B., Burns, D., and Dyall-Smith, M. (2010) Diversity of *Haloquadratum* and other haloarchaea in three, geographically distant, Australian saltern crystallizer ponds. *Extremophiles* **14**: 161–169.

Oksanen, J.F., Blanchet, G., Friendly, M., Kindt, R., Legendre, P., McGlinn, D., *et al*. (2019) vegan: Community Ecology Package. R package version 2.5–6.

Oren, A. (2011) Thermodynamic limits to microbial life at high salt concentrations. *Environ Microbiol* **13**: 1908–1923.

Oren, A. (2013) Life in magnesium- and calcium-rich hypersaline environments: salt stress by chaotropic ions. In

Polyextremophiles, Seckbach, J., Oren, A., and Stanlotter, H. (eds): Dordrecht, Netherlands: Springer, pp. 215–232.

Papke, R.T., Corral, P., Ram-Mohan, N., de la Haba, R.R., Sánchez-Porro, C., Makkay, A., and Ventosa, A. (2015) Horizontal gene transfer, dispersal and haloarchaeal speciation. *Life* **5**: 1405–1426.

Papke, R.T., Koenig, J.E., Rodríguez-Valera, F., and Doolittle, W.F. (2004) Frequent recombination in a saltern population of *Halorubrum*. *Science* **353**: 1928–1930.

Paradis, E., and Schliep, K. (2019) ape 5.0: an environment for modern phylogenetics and evolutionary analyses in R. *Bioinformatics* **35**: 526–528.

Pett-Ridge, J., and Weber, P.K. (in press). NanoSIP: NanoSIMS applications for microbial biology. In *Microbial Systems Biology: Methods and Protocols*, 2nd ed, Navid, A. (ed): Totowa, NJ: Humana Press, pp. 375–408.

Pfaff, J.D. (1993) *Method 300.0: Determination of Inorganic Anions by Ion Chromatography*. Revision 2.1, Cincinnati, OH: U.S. EPA.

Polerecky, L., Adam, B., Milucka, J., Musat, N., Vagner, T., and Kuypers, M.M.M. (2012) Look@NanoSIMS—a tool for the analysis of nanoSIMS data in environmental microbiology. *Environ Microbiol* **14**: 1009–1023.

Popa, R., Weber, P.K., Pett-Ridge, J., Finzi, J.A., Fallon, S. J., Hutcheon, I.D., *et al*. (2007) Carbon and nitrogen fixation and metabolite exchange in and between individual cells of *Anabaena oscillarioides*. *ISME J* **1**: 354–360.

Ram Mohan, N., Fullmer, M.S., Makkay, A.M., Wheeler, R., Ventosa, A., Naor, A., *et al*. (2014) Evidence from phylogenetic and genome fingerprinting analyses suggests rapidly changing variation in *Halorubrum* and *Haloarcula* populations. *Front Microbiol* **5**: 143.

Robinson, J.L., Pyzyna, B., Atrasz, R.G., Henderson, C.A., Morrill, K.L., Burd, A.M., *et al*. (2005) Growth kinetics of extremely halophilic archaea (family Halobacteriaceae) as revealed by Arrhenius plots. *J Bacteriol* **187**: 923–929.

Rodriguez-Brito, B., Li, L., Wegley, L., Furlan, M., Angly, F., Breitbart, M., *et al*. (2010) Viral and microbial community dynamics in four aquatic environments. *ISME J* **4**: 739–751.

Sass, A.M., McKew, B.A., Sass, H., Fichtel, J., Timmis, K.N., and McGenity, T.J. (2008) Diversity of *Bacillus*-like organisms isolated from deep-sea hypersaline anoxic sediments. *Saline Syst* **4**: 8.

Sawyer, W.H., and Puckridge, J. (1973) The dissociation of proteins by chaotropic salts. *J Biol Chem* **248**: 8429–8433.

Selinummi, J., Seppälä, J., Yli-Harja, O., and Puhakka, J.A. (2005) Software for quantification of labeled bacteria from digital microscope images by automated image analysis. *Biotechniques* **39**: 859–862.

Serec, K., Dolanski Babić, S., Podgornik, R., and Tomić, S. (2016) Effect of magnesium ions on the structure of DNA thin films: an infrared spectroscopy study. *Nucleic Acids Res* **44**: 8456–8464.

Stevenson, A., Cray, J.A., Williams, J.P., Santos, R., Sahay, R., Neuenkirchen, N., *et al*. (2015) Is there a common water-activity limit for the three domains of life? *ISME J* **9**: 1333–1351.

Stevenson, A., Hamill, P.G., O'Kane, C.J., Kminek, G., Rummel, J.D., Voytek, M.A., *et al*. (2017) *Aspergillus penicillioides* differentiation and cell division at 0.585 water activity. *Environ Microbiol* **19**: 687–697.

Stryhanyuk, H., Calabrese, F., Kümmel, S., Musat, F., Richnow, H.H., and Musat, N. (2018) Calculation of single cell assimilation rates from SIP-nanoSIMS-derived isotope ratios: a comprehensive approach. *Front Microbiol* **9**: 2342.

Tosca, N.J., Knoll, A.H., and McLennan, S.M. (2008) Water activity and the challenge for life on early Mars. *Science* **320**: 1204–1208.

Walters, W., Hyde, E.R., Berg-lyons, D., Ackermann, G., Humphrey, G., Parada, A., *et al*. (2015) Improved bacterial 16S rRNA gene (V4 and V4-5) and fungal internal transcribed spacer marker gene primers for microbial community surveys. *mSystems* **1**: e0009-15.

Webb, S.J., Rabsatt, T., Erazo, N., and Bowman, J.S. (2019) Impacts of *Zostera* eelgrasses on microbial community structure in San Diego coastal waters. *Elem Sci Anthr* **7**: 11.

Wolery, T.W. and Jarek, R.L. (2003) EQ3/6, version 8.0. Sandia National Laboratories.

Yakimov, M.M., La Cono, V., Spada, G.L., Bortoluzzi, G., Messina, E., Smedile, F., *et al*. (2015) Microbial community of the deep-sea brine Lake Kryos seawater-brine interface is active below the chaotropicity limit of life as revealed by recovery of mRNA. *Environ Microbiol* **17**: 364–382.

Zajc, J., Džeroski, S., Kocev, D., Oren, A., Sonjak, S., Tkavc, R., and Gunde-Cimerman, N. (2014) Chaophilic or chaotolerant fungi: a new category of extremophiles? *Front Microbiol* **5**: 708.

Zeder, M., Kohler, E., and Pernthaler, J. (2010) Automated quality assessment of autonomously acquired microscopic images of fluorescently stained bacteria. *Cytom Part A* **77A**: 76–85.

Zhaxybayeva, O., Stepanauskas, R., Ram Mohan, N., and Papke, R.T. (2013) Cell sorting analysis of geographically separated hypersaline environments. *Extremophiles* **17**: 265–275.

Supporting Information

Additional Supporting Information may be found in the online version of this article at the publisher's web-site:

Appendix S1: Supplementary Information